Journal of Quantitative Spectroscopy & Radiative Transfer 108 (2007) 126–145

Journal of Quantitative Spectroscopy & Radiative Transfer

www.elsevier.com/locate/jqsrt

Collisional parameters of H_2O lines: Velocity effects on the line-shape

H. Tran[a], D. Bermejo[b], J.-L. Domenech[b], P. Joubert[c], R.R. Gamache[d], J.-M. Hartmann[a,*]

[a]*Laboratoire Interuniversitaire des Systèmes Atmosphériques, CNRS (UMR 7583), Universités Paris 7 et Paris 12, 94010 Créteil Cedex, France*

[b]*Instituto de Estructura de la Materia, Consejo Superior de Investigaciones Cientificas, Serrano 123, 28006 Madrid, Spain*

[c]*Institut UTINAM, CNRS (UMR 6213), Université Franche-Comté, 25030 Besançon Cedex, France*

[d]*Department of Environmental, Earth, and Atmospheric Sciences, University of Massachusetts Lowell, 265 Riverside Street, Lowell, MA 01854, USA*

Received 24 January 2007; received in revised form 7 March 2007; accepted 8 March 2007

Abstract

This paper is devoted to the effects of velocity on the shapes of six $R(J)$ lines of the v_3 band of water vapor diluted in N_2. The experiments have been made at room temperature for total pressures between 0.1 and 1.2 atm using a tunable infrared laser frequency difference spectrometer. These measurements, which study broad and narrow lines of low and high J values, are first analyzed using the Voigt and the hard collision (HC) model. It is shown that both lead to unsatisfactory results, the Voigt profile being unable to account for the line narrowing whereas the friction (narrowing) parameter deduced using the HC approach has an unphysical dependence on pressure. Furthermore, at elevated pressure where Dicke narrowing and Doppler effects are negligible, deviations between experimental and fitted profiles are still observed, indicating inhomogeneous effects due to the speed dependence of collisional parameters. In order to go further, an approach based on the kinetic impact equation accounting for both the Dicke narrowing and the speed dependence has been applied. It uses velocity-dependent broadening and shifting coefficients calculated with a semi-classical approach and two parameters. The latter, which govern the memory functions of the modulus and orientation of the H_2O velocity are considered as free parameters and determined from experiments. The results show that all profiles, regardless of pressure and of the transition, can be correctly modeled using a single set of memory parameters. This demonstrates the consistency of the approach, which is then used to analyze the different regimes that monitor velocity effects on the line profile.

Keywords: Water vapor; Line-shape; Velocity effects

1. Introduction

Due to the importance of water vapor in our atmosphere, the broadening and shifting of H_2O absorption lines have been the subject of many experimental and theoretical efforts in the last 20 years (see Refs. [1,2] and

*Corresponding author. Tel.: +33 145176542; fax: +33 145171564.
E-mail address: hartmann@lisa.univ-paris12.fr (J.-M. Hartmann).

0022-4073/$ - see front matter © 2007 Elsevier Ltd. All rights reserved.
doi:10.1016/j.jqsrt.2007.03.009

those cited therein). Deviations of measured H_2O absorption with respect to the Voigt shape have been pointed out a while ago [3], and accounted for or studied in a number of papers [3–20] since then. Nevertheless, for H_2O–N_2 (and air) mixtures, there are, to our knowledge, few works providing large sets of data on the spectral shape for various lines and pressures [18,19]. In Refs. [3–20], a narrowing of the line-shape is observed that mostly affects rovibrational transitions (of high J and K_a or K_c values), which have small broadening coefficients. It is important to note that in most of these studies, this phenomenon has been attributed only to changes of the H_2O velocity induced by collisions (i.e. confinement or Dicke narrowing) and that the eventual participation of the dependence of collisional parameters (width and shift) on the absolute speed of the radiatively active molecule has seldom been considered. To our knowledge, the only studies that consider this effect for H_2O are those of Refs. [18–20]. They conclude that the speed dependence does have an effect but few results are given and, as will be shown here, empirical and approximate speed dependences of the broadening coefficients are used. Note that an indication of the importance of speed averaging of the line-shape can be found in the "strange" results that may be obtained when only the confinement narrowing is considered. Indeed, the friction parameters β deduced from fits of measured absorption then depend on the rovibrational transition and show a non-linear dependence on pressure as demonstrated in this paper and in Ref. [19].

The present paper is the third of a series devoted to the effects of collisions on absorption lines of water vapor diluted in N_2 (and air). After studies of the influence of vibration [1] and temperature [21] on the pressure broadening and shifting coefficients, we now study the influence of velocity changes and velocity averaging on the spectral shape and the resulting deviations from the Voigt profile. The experiments were carried out in Madrid using a tunable infrared laser frequency difference spectrometer. Absorption by water vapor highly diluted in nitrogen was measured at room temperature for nine total pressures between 0.1 and 1.2 atm. The spectral transitions under study are six $R(J)$ lines of the ν_3 band with rotational quantum numbers $K_c = J$ (and $K_a = 0$ or 1). These, for $J = 3$, 5, 8, 10, 12, and 14, were chosen since their collisional broadening decreases rapidly with J [1] showing a ratio of about 10 between the broadest and the narrowest. This leads to very different deviations from the Voigt profile for a given pressure as will be shown latter. Furthermore, as demonstrated in Ref. [21], the temperature dependence of the widths varies largely from low to high J lines. This indicates large differences of the velocity dependence from line to line so that significantly different inhomogeneous effects of the speed averaging are expected.

In order to model the line-shapes, the Keilson and Storer 3-dimensional (KS-3D) approach, recently developed and successfully applied to H_2 Raman transitions [22,23], is used. This is a powerful approach, self consistent for all pressures from the Doppler to the collisional regime, that includes both the confinement narrowing of the Doppler distribution and the radiator speed dependence of the collisional width and shift. In order to do that, the velocity orientation and velocity modulus memory mechanisms are distinctly considered as explained in Ref. [24]. Starting from the impact kinetic equation, including the Doppler contribution with a convenient bi-parametric 3D radiator velocity memory function, the expression for the line shape is established. It is based on two quantities that parameterize the influence of collisions on the orientation γ_{Ori} and modulus γ_{Mod} of the H_2O velocity. Using semi-classical predictions [1,21] of the dependences of the broadening and shift on the relative velocity, the values of γ_{Ori} and γ_{Mod}, that are the only adjustable quantities of the model, are determined in order to get agreement with measurements. It is then demonstrated that, with these two parameters only, all measured profiles are correctly reproduced, regardless of the line and total pressure. The model is then used for the analysis of the different mechanisms that govern the line shape.

2. Experimental, data treatment, and results

2.1. Experiments

Spectra were recorded with the infrared laser frequency difference spectrometer in Madrid [25,26]. For these experiments the Ar^+ laser operated at 514 nm, single-mode, actively frequency stabilized and locked to a $^{127}I_2$ hyperfine transition. The ring dye laser used DCM as dye and was frequency stabilized and scanned using its own (commercial) electronics. The wavenumber scale of each scan was linearized and calibrated a posteriori

using the transmission fringes of a 150 MHz FSR confocal Fabry–Perot interferometer and the tabulated frequencies of the Doppler limited absorption spectrum of I_2 [27].

Mixtures of H_2O vapor and N_2 were prepared in a sample cylinder at least 24 h before the experiments. Bi-distilled water was de-gased, and then allowed to enter the sample cylinder up to the desired amount before 99.995% purity nitrogen was added up to a pressure of about 9 bar. The sample concentrations were chosen for each studied spectral transition in order to have peak transmissions at line centers of the order of 30%. The cell used for the absorption measurement was a 1 m long stainless steel tube with CaF_2 windows mounted parallel to each other at the Brewster angle.

For each of the studied regions the following experimental procedure was used: first an empty cell spectrum was recorded, then the cell was filled at the maximum studied pressure and a second recording was made. Then the cell was partially pumped out and a new spectrum was taken, this procedure being repeated sequentially at nominal pressures close to 1.2, 1.0, 0.8, 0.6, 0.5, 0.4, 0.3, 0.2 and 0.1 atm. Finally, a second empty cell spectrum was taken as a (successful) check of the stability of the system. The transmission of a given gas sample was then deduced from the ratio of the recordings obtained with and without gas in the cell. A few recordings were also made for pure water vapor at a very low pressure (≈ 1 mb) in order to check the potential influence of the finite resolution of the lasers used. This test, carried for three lines near 3947 cm^{-1}, lead to Doppler widths, obtained from Voigt fits of the measured absorptions, only 1% ($\approx 5\times10^{-5}$ cm^{-1}) greater than the theoretical value. Hence, the influence of the instrument line-shape was neglected in all the following analysis.

Absorption of the infrared radiation by water vapor in the laboratory air was significant for the strongest lines under study. The design of the spectrometer precluded encasing it in a box that could be evacuated or flushed with dry nitrogen. Since the instrument has two beams (i.e. the "signal" beam that goes through the sample, and the "reference" beam used to ratio out power fluctuations) it was possible to compensate for the atmospheric absorption by keeping the paths in open air to the exact same length in both beams. However, and particularly for the strongest water lines, atmospheric absorption substantially attenuated the infrared intensity reaching the detectors, decreasing the signal-to-noise ratio. Therefore, most of the optical mounts were modified to fit flexible plastic tubes between them that were purged by a dry nitrogen flow. The only non-purged path in the system was a small gap between the $LiNbO_3$ oven and the Ge filter before the beam-splitter that affected equally both beams and was well compensated. At the peak of the strongest line studied ($4_{0,4}\leftarrow 3_{0,3}$), residual atmospheric absorption was ~50%, which was well ratioed out using the empty cell measurements.

Since absorption/desorption of H_2O on the walls of the sample cylinder and cell was impossible to control and varied with the N_2 pressure and the history of operations, the total amount of water in these sequences is poorly known. Hence, the partial pressure of H_2O was deduced, for each spectrum, from the integrated absorption deduced from the fits of measured spectra and the values of the line intensities tabulated in the HITRAN database [28]. The numbers obtained were then used in order to correct for the contribution of self-broadening (see below).

2.2. Data treatment

When the speed dependence of collisional parameters is disregarded, various models have been proposed in order to describe the confinement narrowed line shape and comparisons between numerous approaches have been made (see Ref. [18] and those therein in the case of H_2O). Hence, and since a different model is used latter in this paper, we have only fitted experiments with the Voigt and the uncorrelated Hard Collision (HC) model of Rautian and Sobel'man, for which the absorption coefficients for a single line are given by

$$\alpha^{\mathrm{Voigt}}(\sigma)=\frac{Sx_{\mathrm{H_2O}}\mathrm{P}}{\sqrt{\pi}}\frac{\sqrt{\ln 2}}{\Gamma_{\mathrm{D}}}\,\mathrm{Re}\{V(\sigma-\sigma_0,\Gamma_{\mathrm{D}},\Delta,\Gamma)\},\tag{1}$$

$$\alpha^{\mathrm{Hard}}(\sigma)=\frac{Sx_{\mathrm{H_2O}}\mathrm{P}}{\sqrt{\pi}}\frac{\sqrt{\ln 2}}{\Gamma_{\mathrm{D}}}\,\mathrm{Re}\left\{\frac{V(\sigma-\sigma_0,\Gamma_{\mathrm{D}},\Delta,\Gamma)}{1-\sqrt{\pi}B(\sqrt{\ln 2}/\Gamma_{\mathrm{D}})V(\sigma-\sigma_0,\Gamma_{\mathrm{D}},\Delta,\Gamma+B)}\right\},\tag{2}$$

where x_{H_2O} is the H_2O mole fraction in the mixture, P is the total pressure and S is the integrated intensity of the line. σ_0 and Γ_D are the unperturbed spectral position of the transition and the Doppler width. Δ, Γ, and B are the pressure-induced line-shift, the (Lorentz) collisional half-width (HWHM), and the narrowing parameter, respectively. The complex probability function V is given by

$$V(\sigma-\sigma_0,\Gamma_D,\Delta,\Gamma)=\frac{\lambda i}{\pi}\int_{-\infty}^{+\infty}\frac{\exp(-t^2)}{(\sigma-\sigma_0-\Delta)(\sqrt{\ln 2}/\Gamma_D)+i\Gamma(\sqrt{\ln 2}/\Gamma_D)-1}\,dt. \tag{3}$$

Note that, at the densities studied here, collisions are binary so that Δ, Γ, and B should show linear variations with total pressure ($\Delta = P\delta$, $\Gamma = P\gamma$, and $B = P\beta$) if the model used is the proper one to represent the observations.

The measured spectra have been least-squares fitted one-by-one with the Voigt approach and, as a test, the other line-shape was applied to some of them. The Doppler width was fixed to the theoretical values since spectra recorded at very low-pressure show no significant broadening due to the instrument function. All lines ℓ of significant absorption in the considered spectra have been fitted simultaneously leading to the determination of S_ℓ, $(\sigma_{0\ell}-\Delta\ell)$, Γ_ℓ (and, eventually, B_ℓ). For high J values, the two doublet lines $(J+1)_{0,J+1}\leftarrow J_{0,J}$ and $(J+1)_{1,J+1}\leftarrow J_{1,J}$ can be very closely spaced (less than $10^{-3}\,cm^{-1}$ for $J=14$); in these cases, the same broadening and shifting parameters were assumed for both transitions, as justified by Ref. [1], while the spectral separation and intensity ratio were fixed to the values given in Ref. [28].

2.3. Results

Fits of the $11_{1,11}\leftarrow 10_{1,10}$ and $11_{0,11}\leftarrow 10_{0,10}$ doublet with the Voigt and HC profiles are shown in Figs. 1 and 2 for the pressures of 0.0973 and 0.497 atm. As expected from previous studies, they demonstrate that the absorption cannot be represented by the Voigt shape whereas the confinement narrowed HC profile of Eq. (2) leads to perfect adjustment of measured data. Nevertheless, the quality of this last fit hides some problems that have been observed previously [18,19]. Indeed, whereas the width Γ and shift Δ are nicely proportional to

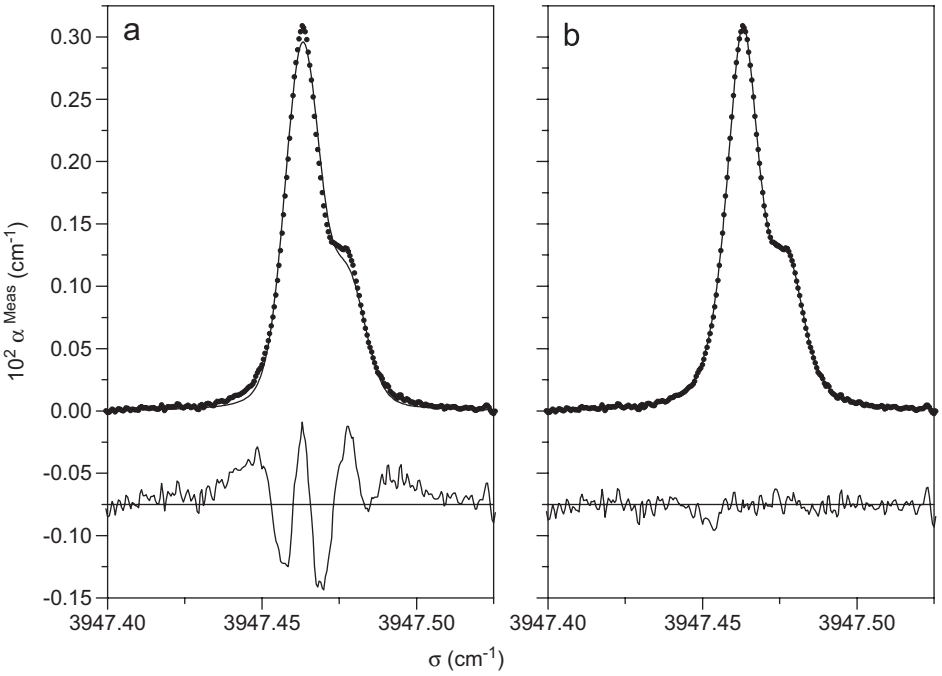

Fig. 1. Absorption coefficient for the $11_{1,11}\leftarrow 11_{1,10}$ and $11_{0,11}\leftarrow 11_{0,10}$ doublet for $P=0.0973$ atm. ● are measured values whereas —— are fitted spectra and $5\times$(Meas-Fit). (a) Results obtained using the Voigt profile and (b) results obtained using the uncorrelated HC model.

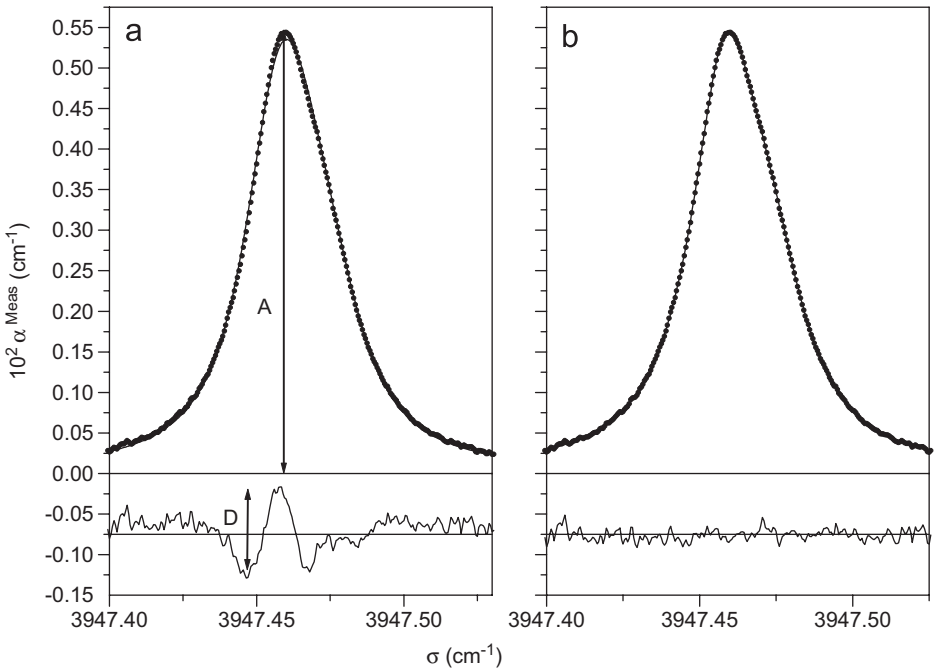

Fig. 2. Absorption coefficient for the $11_{1,11} \leftarrow 11_{1,10}$ and $11_{0,11} \leftarrow 11_{0,10}$ doublet for $P = 0.497$ atm. ● are measured values whereas —— are fitted spectra and $5 \times$ (Meas-Fit). (a) Results obtained using the Voigt profile and (b) results obtained using the uncorrelated HC model.

pressure ($\Gamma = \gamma p$ and $\Delta = \delta p$ within a couple of %), that is not the case of B as shown in Fig. 3. Another indication that models only accounting for confinement narrowing are not fully adapted for the representation of the measured line-shapes is given by the fact that the associated narrowing parameters $\beta = B/p$ depend on the transition [18,19]. This shows that none of the approaches used is adapted for the modeling of the observed data. A further confirmation of this is given by Fig. 4, which corresponds to the broadest line (0.11 cm^{-1}/atm).[1] For the pressures of the figure, although the regime is purely collisional and Doppler and Dicke-type narrowing effects are negligible, a w-shaped signature remains in the observed-fit deviations; its amplitude is almost independent on pressure whereas its width is proportional to the broadening Γ (i.e. to pressure) as shown in Fig. 5. These failures of the models used can thus be attributed to the influence of the speed dependence of the collisional parameters as discussed latter on in this paper.

For all studied transitions, the shifts Δ deduced from fits using the Voigt and HC profiles are consistent and show nice linear variations with pressure (Fig. 3) permitting precise determinations of δ. In the case of the broadening coefficients $\gamma = \Gamma/P$, they all show, with various scales, the relative variations shown in Fig. 3: the values of γ determined using the Voigt line shape increase with P and tend to become constant at elevated pressure even though a small narrowing remains (Fig. 4). In order to carry comparisons with previous measurements, we have determined the "broadening coefficient" γ from this high pressure asymptotic (which is consistent with values derived, for lower pressures, using the HC model as shown in Fig. 3). Since the mixtures studied contain amounts of water vapor (from less than 0.1% to about 2%) that make contributions of H_2O–H_2O collisions to the broadening not always negligible, the results obtained have then been corrected for self broadening using the data of Refs. [28–30]. The pressure broadening and sifting coefficients determined as explained above are compared with previous determinations for the same transitions in Table 1 where measurements for ν_2 lines of "close" rotational quantum numbers are also given. As can be seen, the overall agreement is quite satisfactory and confirms the quality of the present

[1] At elevated pressure, when $\Gamma/\Gamma_D \gg 1$, one can easily show that the HC profile in Eq. (2) tends to the Lorenzian profile so that the influence of B vanished. As a result, accounting for the narrowing observed in Fig. 4 using the HC line-shape leads to values of $\beta = B/P$ that diverge with increasing pressure.

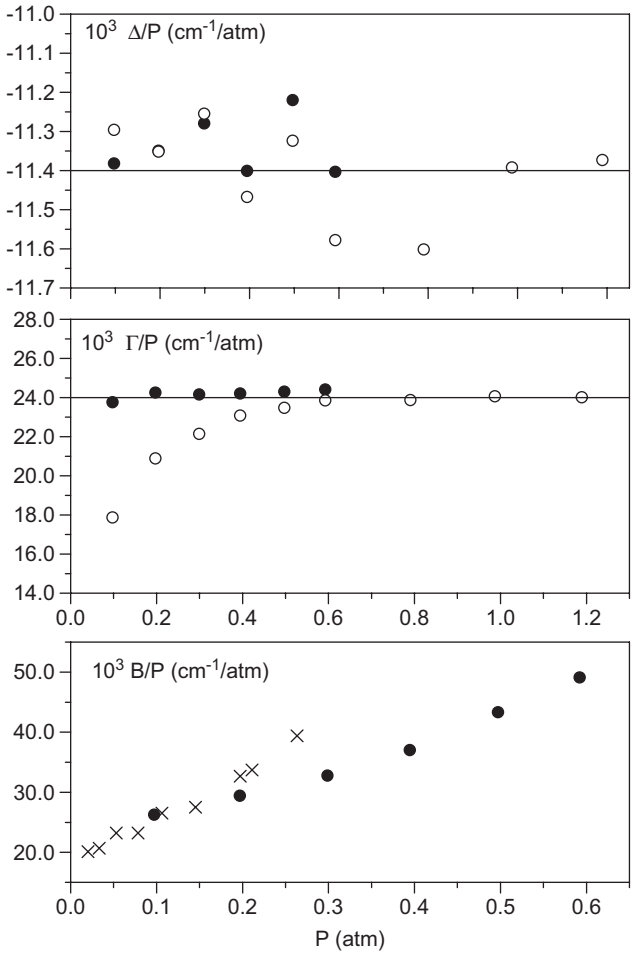

Fig. 3. ● pressure dependence of the collisional parameters obtained from fits of the $11_{1,11} \leftarrow 11_{1,10}$ and $11_{0,11} \leftarrow 11_{0,10}$ doublet using the uncorrelated HC model. ○ are values obtained from fits using the Voigt profile. × are values obtained for the $9_{8,1} \leftarrow 8_{7,2}$ and $9_{8,2} \leftarrow 8_{7,1}$ doublet in Ref. [19].

determinations even though the broadening varies by one order of magnitude from the narrowest to the widest line.

For further analysis and comparisons of measured and calculated profiles, we have retained, from the fit of each spectrum with a Voigt line-shape, two pressure-dependent quantities that quantify the amount of narrowing. The first is the value of Γ/P as plotted in Fig. 3. The second, called W, is the amplitude, relative to line-center absorption, of the "w-type" shape deviation between experimental and fitted profiles ($W = 100D/A$ as indicated in Fig. 2a). As illustrated in Fig. 6, where values are plotted vs. γP for a relative comparison of the behaviors of different lines, significantly different effects are observed depending on the transition, demonstrating the importance of inhomogeneous effects due to the speed dependence of the broadening. Indeed, if all lines had identical dependences (i.e. the same $\gamma(v)/\bar{\gamma}$ or $\gamma(v)/\gamma(\bar{v})$) all values would fall on a single curve. Note that, as discussed latter, these variations of inhomogeneous narrowing from line-to-line could be expected considering the very different evolutions of $\gamma(v)$ (see Ref. [21] and Fig. 7).

Finally, as is well known, the speed dependence of the collisional parameters can result in an asymmetry of the line-shape (e.g., [9,20]), particularly when the pressure-induced shift depends strongly on speed and is significant when compared to broadening. Nevertheless, careful consideration of the residuals of the fit shows that, within experimental errors, the measured profiles of the lines under study here are symmetric.

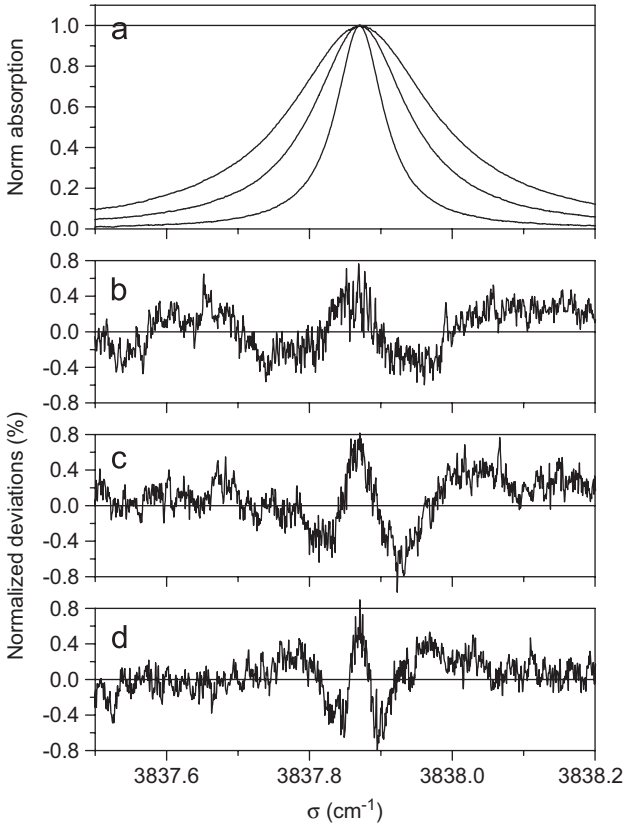

Fig. 4. Absorption by the $4_{0,4} \leftarrow 3_{0,3}$ line and deviations from fits with a Voigt profile. (a) Peak normalized measured absorptions for pressures of about 1.2, 0.8, and 0.4 atm and (b)–(d) are deviations relative to peak absorption for the pressures 1.2, 0.8, and 0.4 atm, respectively.

3. Model for velocity effects on the line profile

In order to take into account all velocity effects (the collisional confinement narrowing of the Doppler distribution and the radiator speed dependence of the collisional broadening and shifting parameters), the numerical KS-3D model developed by Bonamy et al. [22–24,36] is used. Since details can be found in these references, only the main points are given here.

3.1. Speed dependence of collisional parameters

The simplest description of the dependence of the broadening parameter on the relative speed $\|\vec{v}_r\|$—between H_2O and N_2—is obtained assuming both resonant collisions and a single component (in $1/R^q$ where R is the intermolecular distance) of the anisotropic interaction potential. In this simple case, the Lorentz half width can be written as [37][2]

$$\gamma(x_r) = A x_r^p, \quad \text{with } p = \frac{q-3}{2(q-1)}, \tag{4}$$

where $x_r = \mu\|\vec{v}_r\|^2/2k_BT$, μ being the reduced mass of the collisional pair. This expression is convenient since the averaging of γ over the Boltzmann distribution of the perturber velocity $\vec{v}_2$ is then straight forward leading to a dependence $\gamma(\|\vec{v}_1\|)$ on the H_2O absolute velocity given by a confluent hypergeometric function depending

[2]Note that although a similar power law can also be used for the shifts, it has no physical signification, except when δ is entirely due to vibrational dephasing.

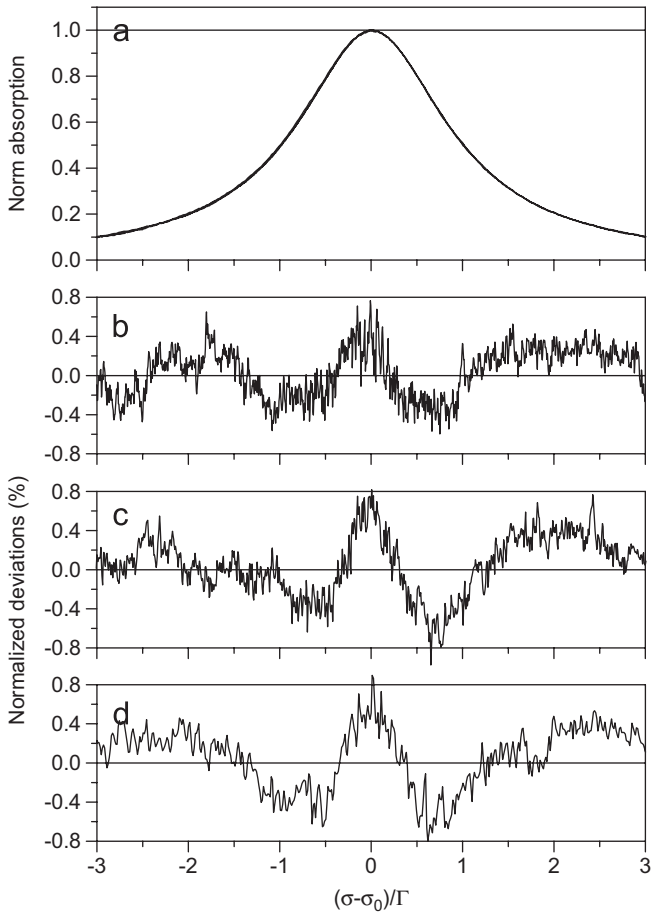

Fig. 5. Same as Fig. 4 except that values are plotted vs. $(\sigma-\sigma_0)/\Gamma$ so that a broadening normalized scale is used leading to identical widths for all lines.

on A and p (or q) [37]. Such an approach has generally been used in the papers where the velocity dependence has been addressed (e.g., [18–20]). In these papers, q is fixed or considered as a free parameter that is adjusted on the measured profiles. Such an approach is reasonable for N_2 broadened H_2O low J transitions since they involve quasi-resonant long-range collisions dominated by the strong dipole–quadrupole interactions. In this case ($q = 4$) so that γ is proportional to $\|\vec{v}_r\|^{1/3}$ (thus leading to the usual $T^{-0.8}$ dependence). Nevertheless, as shown in Ref. [21] where very different temperature dependences (e.g. from $T^{-0.8}$ to $T^{+0.2}$) have been observed, this simple approach breaks down as J increases. It is particularly the case for high J lines whose broadenings result from very non-resonant collisions and interactions at short distance where different contributions to the potential are simultaneously significant. This is shown in Fig. 7 where values have been calculated using the model of Refs. [1,21] indicating that Eq. (4) is clearly insufficient since it would require values of p that depend on $\|\vec{v}_r\|$ and on the transition. Furthermore, p greater than 1/2 can only be obtained assuming unphysical interaction potentials (e.g., $p = 1$ corresponds to $q = -1$). In order to be able to correctly represent all broadenings and shiftings, a more flexible three parameter analytical law is used here, i.e.:

$$\gamma(x_r) = A x_r^p \exp(-c x_r) \quad \text{and} \quad \delta(x_r) = A' x_r^{p'} \exp(-c' x_r). \tag{5}$$

When this equation is used, the Boltzmann average over the collision partner (N_2) velocity distribution is still analytical although more complicated than when Eq. (4) is used [23], leading to the following dependence

Table 1
Measured broadening and shifting coefficients of H_2 ^{16}O ν_3 lines by N_2

	δ (10^{-3} cm^{-1}/atm)[a]	γ (10^{-3} cm^{-1}/atm)[a]
$4_{0\,4} \leftarrow 3_{0\,3}$ (3837.869 cm^{-1})	1.8±0.1 [present]	101.7±0.5 [present]
	1.1±0.1 [31]	95.6±0.6 [31]
	0.8±0.1 [29][b]	102.0±3.0 [29][b]
"Similar" transitions	γ (10^{-3} cm^{-1}/atm)[c]	γ (10^{-3} cm^{-1}/atm)[c]
	$4_{1\,4} \leftarrow 3_{0\,3}$	$4_{0\,4} \leftarrow 3_{1\,3}$
	114.4±0.6 [32]	99.6±0.8 [15]
	104.5±2.0 [15]	103.3±0.50 [32]
	102.1±2.8 [29][b]	97.4±2.71 [29][b]
	103.4±5.0 [15][b]	98.2±1.0 [15][b]
	109.3±0.3 [32][b]	99.3±0.2 [32][b]
	103.4±2.0 [21][b]	99.3±2.0 [21]
$6_{0\,6} \leftarrow 5_{0\,5}$ (3870.129 cm^{-1})	−1.3±0.1 [present]	81.5±1.0 [present]
	−1.35±0.13 [31]	77.8±0.4 [31]
	−2.30±0.35 [29][b]	81.2±2.5 [29][b]
"Similar" transitions	γ (10^{-3} cm^{-1}/atm)[c]	γ (10^{-3} cm^{-1}/atm)[c]
	$6_{0\,6} \leftarrow 5_{1\,5}$	$6_{1\,6} \leftarrow 5_{0\,5}$
	77.2±6.0 [33]	
	79.9±0.7 [15]	82.0±2.5 [15]
	80.4±1.3 [32]	90.20±1.6 [32]
	76.26±2.1 [29][b]	80.0±2.0 [15][b]
	77.8±0.3 [32][b]	80.2±2.2 [29][b]
	77.9±1.5 [15][b]	86.1±0.3 [32][b]
	78.4±1.6 [21][b]	82.6±1.7 [21][b]
$9_{1\,9} \leftarrow 8_{1\,8}$ (3917.286 cm^{-1}) $9_{0\,9} \leftarrow 8_{0\,8}$	−8.4±0.5 [present]	43.0±0.8 [present]
	−7.8±0.4 [31]	39.8±1.0 [31]
	−7.7±0.4 [31]	41.0±0.6 [31]
	−9.5±1.4 [29][b]	40.7±1.1 [29][b]
"Similar" transitions	γ (10^{-3} cm^{-1}/atm)[c]	γ (10^{-3} cm^{-1}/atm)[c]
	$9_{0\,9} \leftarrow 8_{1\,8}$	$9_{1\,9} \leftarrow 8_{0\,8}$
	40.7±0.4 [15]	40.7±0.4 [15]
	39.8±1.2 [29][b]	39.5±1.1 [29][b]
	40.7±1.2 [15][b]	40.2±1.0 [15][b]
	40.3±0.8 [21][b]	39.8±0.8 [21][b]
$11_{1\,11} \leftarrow 10_{1\,10}$ (3947.463 cm^{-1}) $11_{0\,11} \leftarrow 10_{0\,10}$	−11.4±0.2 [present]	24.0±0.5 [present]
	−11.3±1.7 [29][b]	23.8±0.9 [29][b]
	−12.3±1.9 [29][b]	26.7±0.7 [29][b]
"Similar" transitions	γ (10^{-3} cm^{-1}/atm)[c]	γ (10^{-3} cm^{-1}/atm)[c]
	$11_{0\,11} \leftarrow 10_{1\,10}$	$11_{1\,11} \leftarrow 10_{0\,10}$
	24.0±1.5 [15]	23.4±0.6 [29][b]
	23.0±0.6 [29][b]	24.2±2.5 [15][b]
	24.2±1.0 [15][b]	47.0±1.5 [35][b]
	47.0±1.5 [35][b]	
$13_{1\,13} \leftarrow 12_{1\,12}$ (3976.263 cm^{-1}) $13_{0\,13} \leftarrow 12_{0\,12}$	−13.2±0.3 [present]	14.4±1.0 [present]
"Similar" transitions	γ (10^{-3} cm^{-1}/atm)[c]	γ (10^{-3} cm^{-1}/atm)[c]
	$13_{0\,13} \leftarrow 12_{1\,12}$	$13_{1\,13} \leftarrow 12_{0\,12}$
	13.5±0.7 [15]	13.4±0.7 [29][b]
	13.6±0.5 [15][b]	13.8±0.5 [15][b]
	13.8±0.4 [29][b]	14.2±0.1 [34][b]
	14.0±0.1 [34][b]	19.7±1.5 [35][b]
	19.7±1.5 [35][b]	
$15_{1\,15} \leftarrow 14_{1\,14}$ (4003.589 cm^{-1}) $15_{0\,15} \leftarrow 14_{0\,14}$	−12.4±1.0 [present]	8.9±1.0 [present]

Table 1 (*continued*)

"Similar" transitions	γ (10^{-3} cm^{-1}/atm)[c]	γ (10^{-3} cm^{-1}/atm)[c]
	$15_{0\,15} \leftarrow 14_{1\,14}$	$15_{1\,15} \leftarrow 14_{0\,14}$
	8.9 ± 0.3 [15]	4.7 ± 1.01 [35][b]
	9.5 ± 0.2 [18]	8.6 ± 0.01 [34][b]
	4.7 ± 1.0 [35][b]	8.8 ± 1.0 [4][b]
	8.6 ± 0.01 [34][b]	
	8.8 ± 1.0[4][b]	9.9 ± 0.7 [15][b]
	9.9 ± 0.7 [15][b]	

[a]Values for the $(J+1)_{1,J+1} \leftarrow J_{1,J}$ and/or $(J+1)_{0,J+1} \leftarrow J_{0,J}$ of the v_3 band.
[b]Indicate measurements for H_2O-air mixtures whose broadening has been converted to N_2 broadening using a 1.1 multiplicative factor [1,21].
[c]Values for the $(J+1)_{1,J+1} \leftarrow J_{0,J}$ transitions of the v_2 band.

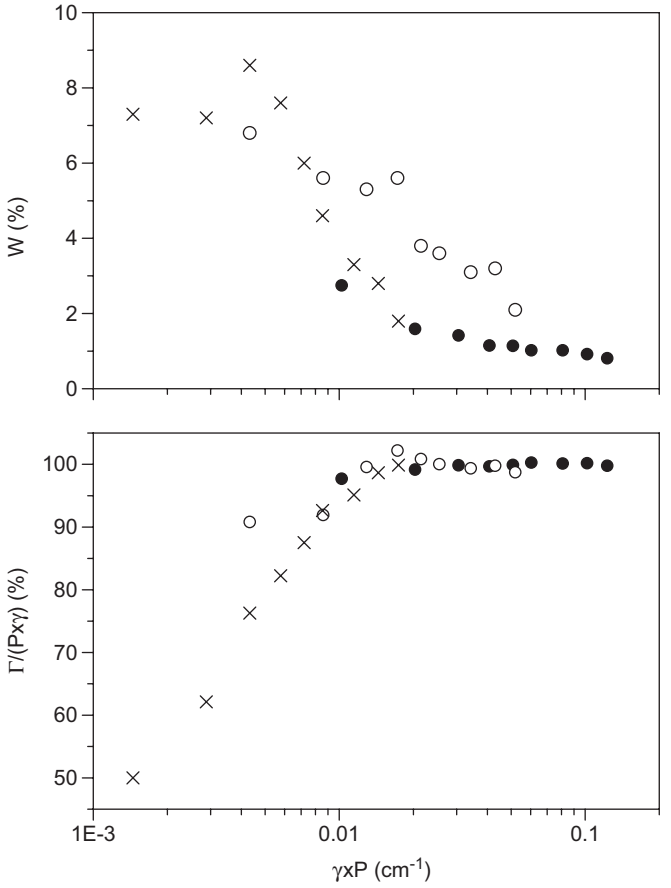

Fig. 6. Measured line shape parameters Γ and W for the ● $R(3)$, ○ $R(8)$, and × $R(12)$ lines.

on the H_2O velocity [$x_1 = \mu\|\vec{v}_1\|^2/2kT$], e.g. in the case of broadening:

$$\gamma(x_1) = \sum_{n=0}^{\infty} \frac{n!\Gamma_{\text{funct}}(3/2)[\mu/m_{H_2O}]^n}{\Gamma_{\text{funct}}(n+3/2)} L_n^{1/2}(x_1)\gamma^{(n)}, \tag{6}$$

with

$$\gamma^{(n)} = \frac{1}{\Gamma_{\text{funct}}(3/2)} \int_0^{\infty} \mathrm{d}x_r \gamma(x_r) x_r^{1/2} \mathrm{e}^{-x_r} L_n^{1/2}(x_r), \tag{7}$$

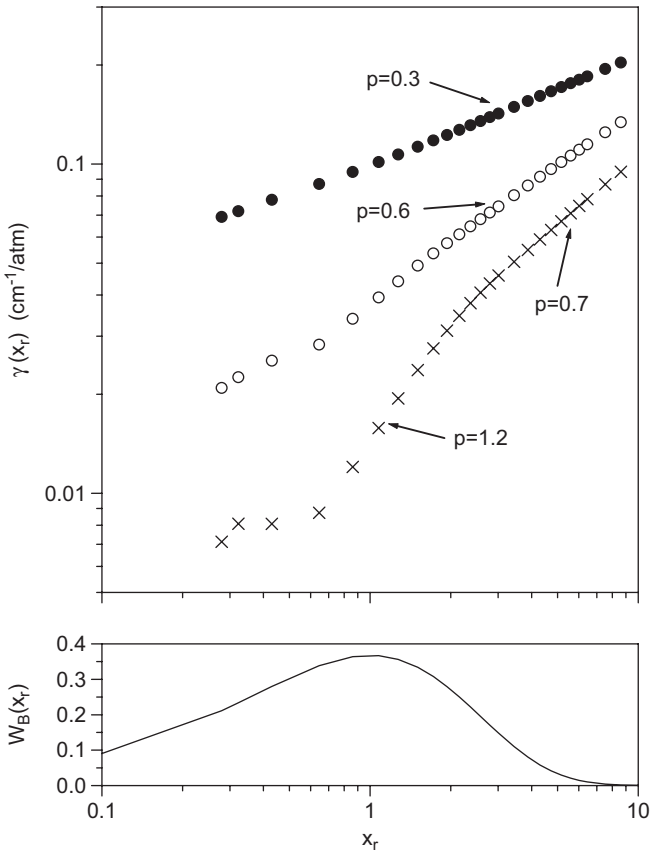

Fig. 7. The top panel displays the dependence of broadening parameters on relative velocity calculated with the semi classical model of Ref. [1] for the lines: ● $R(3)$, ○ $R(8)$, × $R(12)$. The lower panel gives the Boltzmann probability distribution of the relative velocity at room temperature.

where $L_n^{1/2}(x)$ are the Laguerre polynomials and the gamma function Γ_{funct}, not to be confused with the broadening, is given by

$$\Gamma_{\text{funct}}(x) = \int_0^\infty t^{x-1} e^{-t}\, dt, \quad \text{for} \quad x > 0.$$

Note that, for practical calculations, the $\gamma(n)$ parameters can be obtained from recurrence relations [38], i.e.:

$$(1+c)n\gamma^{(n)} = [n-1-p+c(2n-1/2)]\gamma^{(n-1)} - c(n-1)\gamma^{(n-2)}, \tag{8}$$

with the following initial values:

$$\gamma^{(0)} = A\frac{\Gamma_{\text{funct}}(p+3/2)}{\Gamma_{\text{funct}}(3/2)}(1+c)^{-p-3/2},$$
$$\gamma^{(1)} = \gamma_0\frac{-c/2-p}{1+c}. \tag{9}$$

3.2. Keilson–Storer model and resulting lines hape

The lines shapes accounting for velocity effects are calculated starting from the kinetic equation for the radiating dipole $d(\vec{v}_1, t)$ [22,39]:

$$\frac{\partial}{\partial t} d(\vec{v}_1, t) = -v^{VC}\left[d(\vec{v}_1, t) - \int d\vec{v}_1' f(\vec{v}_1', \vec{v}_1) d(\vec{v}_1', t)\right] - \left[i\vec{k}.\vec{v}_1 + \gamma(\vec{v}_1) + i\delta(\vec{v}_1)\right] d(\vec{v}_1, t), \tag{10}$$

where v^{VC} is the velocity changing (VC) collision frequency. $f(\vec{v}_1', \vec{v}_1)$ is the radiator velocity memory function describing the probability per unit time of collisions involving a velocity change $\vec{v}_1' - \vec{v}_1$ and $\vec{k}$ is the radiation vector, $\gamma(\vec{v}_1)$ and $\delta(\vec{v}_1)$ are the velocity-dependent collisional broadening and shifting coefficients. In the model of Refs. [36,40], the $f(\vec{v}_1', \vec{v}_1)$ memory function is given by

$$f(\vec{v}_1', \vec{v}_1) = (1 - \gamma_{Coll}^2)^{-3/2} W_B\left(\frac{\vec{v}_1 \gamma_{Coll} \vec{v}_1'}{\sqrt{1 - \gamma_{Coll}^2}}\right), \tag{11}$$

where $W_B(x) = (2/\sqrt{\pi})e^{-x}\sqrt{x}$ is the equilibrium Boltzmann distribution. γ_{Coll}, which is the unique parameter of this approach, characterizes the strength of inelastic collisions when $\gamma_{Coll} = 0$, $f(\vec{v}_1', \vec{v}_1) = W_B(\vec{v}_1')$, and the radiator velocity is thermalized after each collision. On the opposite, when $\gamma_{Coll} = 1$, $f(\vec{v}_1', \vec{v}_1) = \delta(\vec{v}_1 - \vec{v}_1')$, so that the radiator velocity remains unchanged after each collision. In Ref. [36], such a parameter governing only the memory of the modulus of $\vec{v}_1$ was introduced in order to model the speed memory effects in the collisional regime, the velocity orientation memory effects being neglected. In order to model the line shape at all pressures, from the Doppler to the collisional regime, the memories of both the modulus and orientation of $\vec{v}_1$ have to be considered. In order to separate the influences of modulus and orientation, Eq. (11) can be rewritten as

$$f(\vec{v}_1', \vec{v}_1)\mathrm{d}\vec{v}_1 = \frac{1}{2\pi} f(x_1', x_1, u)\mathrm{d}x_1\,\mathrm{d}u\,\mathrm{d}\varphi, \tag{12}$$

with

$$f(x_1', x_1, u) = \frac{W_B(x_1)}{2(1 - \gamma_{Coll}^2)^{3/2}} \exp\left[-(1 - \gamma_{Coll}^2)^{-1}\left(\gamma_{Coll}^2(x_1 + x_1') - 2\gamma_{Coll} u\sqrt{x_1 x_1'}\right)\right], \tag{13}$$

where $x_1 = m_1\|\vec{v}_1\|/2kT$ (and x_1') define the speeds whereas $u = \cos(\vec{v}_1', \vec{v}_1)$ and φ parameterize the orientation. The $f(x_1', x_1, u)$ function can be developed on the $P_\ell(u)$ Legendre polynomial basis as

$$f(x_1', x_1, u) = \frac{1}{2}\sum_{\ell=0}^{\infty} f_\ell(x_1', x_1) P_\ell(u), \tag{14}$$

where we can find the solution for $f_\ell(x_1', x_1)$ from Eq. (13) and Eq. (10.2.36) of Ref. [38]:

$$f_\ell(x_1', x_1) = W_B(x_1)(x_1 x_1')^{\ell/2} \sum_{n=0}^{\infty} \frac{n!\Gamma(3/2)\gamma^{2n+\ell}}{\Gamma_{funct}(n + \ell + 3/2)} L_n^{\ell+1/2}(x_1) L_n^{\ell+1/2}(x_1'). \tag{15}$$

The velocity modulus memory function is then obtained by a pertinent orientation averaging

$$f_{Mod} = (x_1', x_1) = \int_{-1}^{1} f(x_1', x_1, u)\,\mathrm{d}u = W_B(x_1) \sum_{n=0}^{\infty} \gamma_{Coll}^{2n} \bar{L}_n^{1/2}(x_1) \bar{L}_n^{1/2}(x_1'), \tag{16}$$

where $\bar{L}_n^{1/2}(x)$ normalized Laguerre polynomials [36], whereas the velocity orientation function can be deduced through the average of x_1

$$f_{Ori}(\vec{v}_1'^{\,0}, \vec{v}_1^{\,0}) = \int_0^{\infty} f(x_1', x_1, u)\,\mathrm{d}x_1 = \frac{1}{2\pi}\sum_{\ell=0}^{\infty} \frac{1}{2}(2\ell + 1)\gamma_{Coll}^{\ell} P_\ell(u), \tag{17}$$

where $\vec{v}_1^{\,0}$ and $\vec{v}_1'^{\,0}$ define the directions.

As mentioned above and demonstrated in Refs. [22,24], such an approach with only one parameter γ_{Coll} governing both the velocity modulus and orientation memories is insufficient when broad pressure ranges, including the Doppler and collisional regimes, are considered. An uncorrelated bi-parametric velocity-memory model was then developed, in which $f(\vec{v}_1', \vec{v}_1)$ is written as the product of memory functions for both orientation and speed [22]:

$$f(x_1', x_1, u) = f_{Mod}(x_1', x_1) f_{Ori}(u) = f_{Mod}(x_1', x_1) f_{Ori}(\vec{v}_1'^{\,0}, \vec{v}_1^{\,0}), \tag{18}$$

where the modulus and the orientation are now characterized by two distinct parameters $\gamma_{\rm Mod}$ and $\gamma_{\rm Ori}$ respectively, so that $\gamma_{\rm Coll}$ is changed to $\gamma_{\rm Mod}$ in Eq. (16) and to $\gamma_{\rm Ori}$ in Eq. (17). They take values between zero and unity, these limiting cases corresponding to instant changes (complete thermalization after one collision) and infinite memory (no changes due to collisions), respectively.

The radiation dipole can then be expanded over the normalized eigenfunctions $Y_{\ell,m}(\vec{v}^0)\bar{L}_n^{1/2}(x)$ [22,38,41]

$$\mathrm{d}(\vec{v}_1,t) = W_{\rm B}(x_1)\sum_{n,\ell,m} a_{n,\ell,m}(t)\,Y_{\ell,m}(\vec{v}_1^0)\bar{L}_n^{1/2}(x_1). \tag{19}$$

From Eqs. (10) and (19), the components $a_{n,\ell,m}(t)$ are given by the differential equation [22]:

$$\dot{a}_{n,\ell,m}(t) + \mathrm{i}\Delta\omega_{\rm D}\left[C_{\ell+1,m}\sum_{n'=0}^{\infty} I_{nn'}a_{n',\ell+1,m}(t) + C_{\ell,m}\sum_{n'=0}^{\infty} I_{nn'}a_{n',\ell-1,m}(t)\right] + v^{\rm VC}\left(1-\gamma_{\rm Mod}^{2n}\gamma_{\rm Ori}^{\ell}\right)a_{n,\ell,m} + \sum_{n'=0}^{\infty}\Gamma_{nn'}a_{n',\ell,m}(t) = 0, \tag{20}$$

where $\Delta\omega_{\rm D} = (\sigma_0/c)\sqrt{2kT/m_a}$ is the Doppler with, $C_{\ell,m} = \sqrt{(\ell^2-m^2)/(2\ell-1)(2\ell+1)}$, and

$$I_{nn'} = \int_0^{\infty} \mathrm{d}x_1\, W_{\rm B}(x_1)\bar{L}_n^{1/2}(x_1)x_1^{1/2}\bar{L}_{n'}^{3/2}(x_1),$$
$$\Gamma_{nn'} = \int_0^{\infty} \mathrm{d}x_1\, W_{\rm B}(x_1)\bar{L}_n^{1/2}(x_1)[\gamma(x_1)+\mathrm{i}\delta(x_1)]\bar{L}_{n'}^{1/2}(x_1), \tag{21}$$

in which the speed dependences of the broadening $\gamma(x_1)$ and shifts $\delta(x_1)$ now appear. The line profile corresponding to the equilibrium distribution in Eq. (19), defined by the Laplace transform of $\mathrm{d}(t) = \int \mathrm{d}\vec{v}\,\mathrm{d}(\vec{v},t)$, is given by

$$\alpha(\Delta\sigma) = \frac{1}{\pi}\mathrm{Re}\{\mathrm{d}\Delta\sigma\} = \frac{1}{\pi}\,\mathrm{Re}\left\{\int_0^{\infty} t\mathrm{e}^{\mathrm{i}\Delta\sigma t}\,\mathrm{d}(t)\,\mathrm{d}t\right\} = \frac{1}{\pi}\mathrm{Re}\{a_{0,0,0}(\Delta\sigma)\}, \tag{22}$$

$\Delta\sigma = \sigma - \sigma_0$ being the distance to the line center wavenumber. Eq. (20) can be written in a condensed form as

$$\dot{a}_{n\ell}(t) = \sum_{\substack{\ell'=\ell\\ \ell'=\ell+1}}\sum_{n'=0}^{\infty}\mathbf{W}_{nn'}^{(\ell,\ell')}a_{n'\ell'}(t) = 0, \tag{23}$$

with

$$\mathbf{W}_{nn}^{(\ell,\ell)} = \left[v^{\rm VC}(1-\gamma_{\rm Mod}^{2n}\gamma_{\rm Ori}^{\ell})\delta_{nn'} + \Gamma_{nn'}\right],$$
$$\mathbf{W}_{nn}^{(\ell,\ell+1)} = \mathrm{i}\Delta\omega_{\rm D}C_{\ell+1}I_{nn'},$$
$$\mathbf{W}_{nn}^{(\ell,\ell-1)} = \mathrm{i}\Delta\omega_{\rm D}C_{\ell}I_{nn'}. \tag{24}$$

In Eqs. (23) and (24) the m index is omitted since the $\mathbf{W}$ matrix is diagonal in m and that only the $m=0$ component is implied in the calculation of the spectral line profile (Eq. (22)). The Laplace transform of Eq. (23) is then

$$(-\mathrm{i}\Delta\sigma + \mathbf{W})a(\Delta\sigma) = 1_{00},$$

where the initial condition $\mathbf{a}(t=0) = \mathbf{1}_{00}$ (or $a_{n,\ell,m}(t=0) = \delta_{n,0}\delta_{\ell,0}\delta_{m,0}$) has been used. Together with Eq. (22) this leads to

$$\alpha(\Delta\sigma) = \frac{1}{\pi}\mathrm{Re}\left\{[-\mathrm{i}\Delta\sigma + \mathbf{W}]^{-1}\right\}_{00}.$$

Note that the resulting line profile can be calculated efficiently diagonalizing $\mathbf{W}$ ($\mathbf{W} = SDS^{-1}$ where D is diagonal), i.e.:

$$\alpha(\Delta\sigma) = \frac{1}{\pi}\,\mathrm{Re}\left\{\sum_q \frac{S_{0,q}(S^{-1})_{q,0}}{-\mathrm{i}\Delta\sigma + D_q}\right\}. \tag{25}$$

3.3. Collisional parameters used

The values of $\gamma(\|\vec{v}_r\|)$ and $\delta(\|\vec{v}_r\|)$ for the transitions under study here have been calculated using the model presented in Refs. [1,21]. As shown in these references, these predictions, made without any adjustable parameters, leads to satisfactory results, except for the highest J lines. This is likely due to uncertainties on the short range potential and/or the breakdown of the semi-classical approach for these transitions, which involve very non-resonant and close collisions. In order to carry comparisons with measurements, these data have first been fitted using Eq. (5) leading to the parameters A, p, and c permitting calculation of $\gamma(x_1)$ and $\delta(x_1)$ through Eqs. (6)–(9). The dependence on $\|\vec{v}_r\|$ (i.e. the parameters p and c for each line) are then kept fixed but the amplitude A is adjusted so that the calculated values, after Boltzmann averaging over $\|\vec{v}_r\|$, match the experimental determinations given in Table 1. Besides these parameters, the numerical calculation of the line shape also requires knowledge of the VC frequency ν^{VC}. Its value was fixed and set equal to:

$$\nu^{VC} = \beta = \frac{k_B T}{2\pi m_1 D_{1-2}}, \tag{26}$$

where the mass diffusional constant of water vapour in nitrogen D_{1-2} was calculated according to Ref. [42].

4. Results and discussion

At this step, all quantities needed for direct calculation of the line shapes are known, except for the memory parameters γ_{Mod} and γ_{Ori}. Their values have been deduced through "manual" tries in order to obtain good agreement between the predicted line profiles and experiment. Note that no least-squares minimization was used due to the high complexity of its implementation so that the values $\gamma_{Ori} = 0.69$ and $\gamma_{Mod} = 0.90$ obtained are only close to the best ones. Note that the velocity modulus memory parameter γ_{Mod} is close to unity (infinite memory limit), indicating strong speed inhomogeneous effects [22,23]. As observed for hydrogen mixtures, the orientation parameters γ_{Ori} is lower than γ_{Mod} but, contrary to previous results obtained for H_2–X systems (X≡Ar or N_2) [22,24], γ_{Ori} and γ_{Mod} are relatively close together. This is probably due to the significantly lower mass ratio between the perturber (N_2) and the active species (H_2O) when compared to systems such as H_2–Ar. In fact, where few collisions with a much heavier collision partner are needed to randomize the velocity orientation of the active molecule induce, this is not the case for light perturbers.

Using these parameters and the velocity dependences of the collisional parameters (Section 3.3) spectra are then calculated according to Section 3.2 under the exact same pressure and temperature conditions as those of the experiments. As for the measurements, these theoretical profiles are fitted using a Voigt shape and the collisional broadening Γ and narrowing signature W are determined exactly as done while treating the measured spectra and described in Sections 2.2 and 2.3.

Comparisons between the values of $\Gamma/(\gamma P)$ and W obtained from experiment and from spectra calculated by using the KS-3D model are plotted in Fig. 8. Uncertainties are not reported for legibility of the plot but those on $\Gamma/(\gamma P)$ are typically of less than a % at the highest pressure to a couple of percent at le lowest pressure for the $R(3)$ line, those for the $R(12)$ transition ranging from about 1% (1.2 atm) to about 10% (0.1 atm). The relative uncertainties on W depend on the transition but they are typically of a few %. These values and the results in Fig. 8 demonstrate the consistency and quality of the model, except for the $R(14)$ line. Indeed, it enables correct description (partially within the uncertainty) of the line-shape under a large variety of conditions involving significantly different velocity effects. The failure in the case of the $R(14)$ transition, besides insufficiencies of the semi-classical model [1,21], is largely due to the significant contribution of self broadening for this weak transition. Indeed, the measurements were made with about 2% of water so that the contribution of H_2O–H_2O collisions ($\gamma_{self} \approx 0.15\,cm^{-1}/atm$, $\gamma_{N2} \approx 0.01\,cm^{-1}/atm$) to the half-width is about 30%. This self-broadening contribution, which is much smaller for the other transitions, significantly reduces the narrowing effects so that the comparison with calculated values in Fig. 8 is not relevant. A proper treatment would require accounting for the effects of H_2O–H_2O interactions, thus introducing the relevant memory parameters and the speed-dependent self-broadening and shifting.

As shown in the case of H_2 diluted in N_2 [22], at high densities the velocity modulus memory parameter γ_{Mod} plays an important role. This is expected since the Doppler effect is weak making the influence of γ_{Ori}

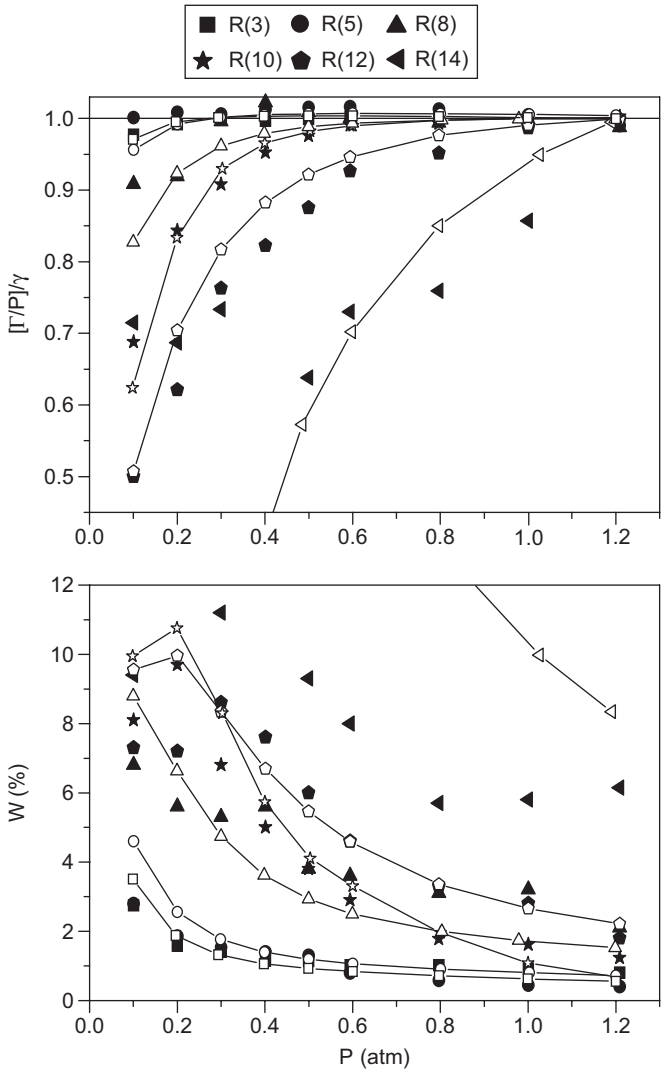

Fig. 8. Comparison between the values of $(\Gamma/P)/\gamma$ and W obtained from experimental (full symbols) and KS-3D calculated spectra (line and open symbols). The values of velocity orientation and modulus memory parameters are $\gamma_{Ori} = 0.69$, $\gamma_{Mod} = 0.90$, respectively.

negligible. Deviations with respect to the Voigt profile are then entirely due to the inhomogeneous speed dependence of collisional parameters whose influence of the profile is governed by γ_{Mod}. In the opposite case corresponding to Dicke and Doppler (low pressure) regimes, collisional broadening and shifting (and thus γ_{Mod}) have small influence whereas the velocity orientation memory parameter γ_{Ori} governs the profile through the confinement reduction of the Doppler broadening. These conclusions are fully confirmed by the results shown in Figs. 9 and 10 for the line $R(12)$ at 0.1 and 2 atm, respectively. Qualitatively similar results are obtained for other lines although they quantitatively depend on the value of $\gamma(v)$: schematically, the results are shifted towards higher (resp. lower) pressures as J increases (resp. decreases). Note that, if these plots indicate that γ_{Mod} and γ_{Ori} have negligible effects in the low- and high-pressure asymptotic regimes, they show that both are needed for pressures in the atmospheric domain.

Finally, recall that, when $\gamma_{Ori} = 1$ and $\gamma_{Mod} = 1$, collisions do not change the velocity (soft collision limit, infinite memory). The KS-3D model leads to a speed-dependent Voigt profile that reduces to a purely Voigt profile if the dependence of γ and δ on v are disregarded and the averaged values $\langle \gamma(v) \rangle$ and $\langle \delta(v) \rangle$

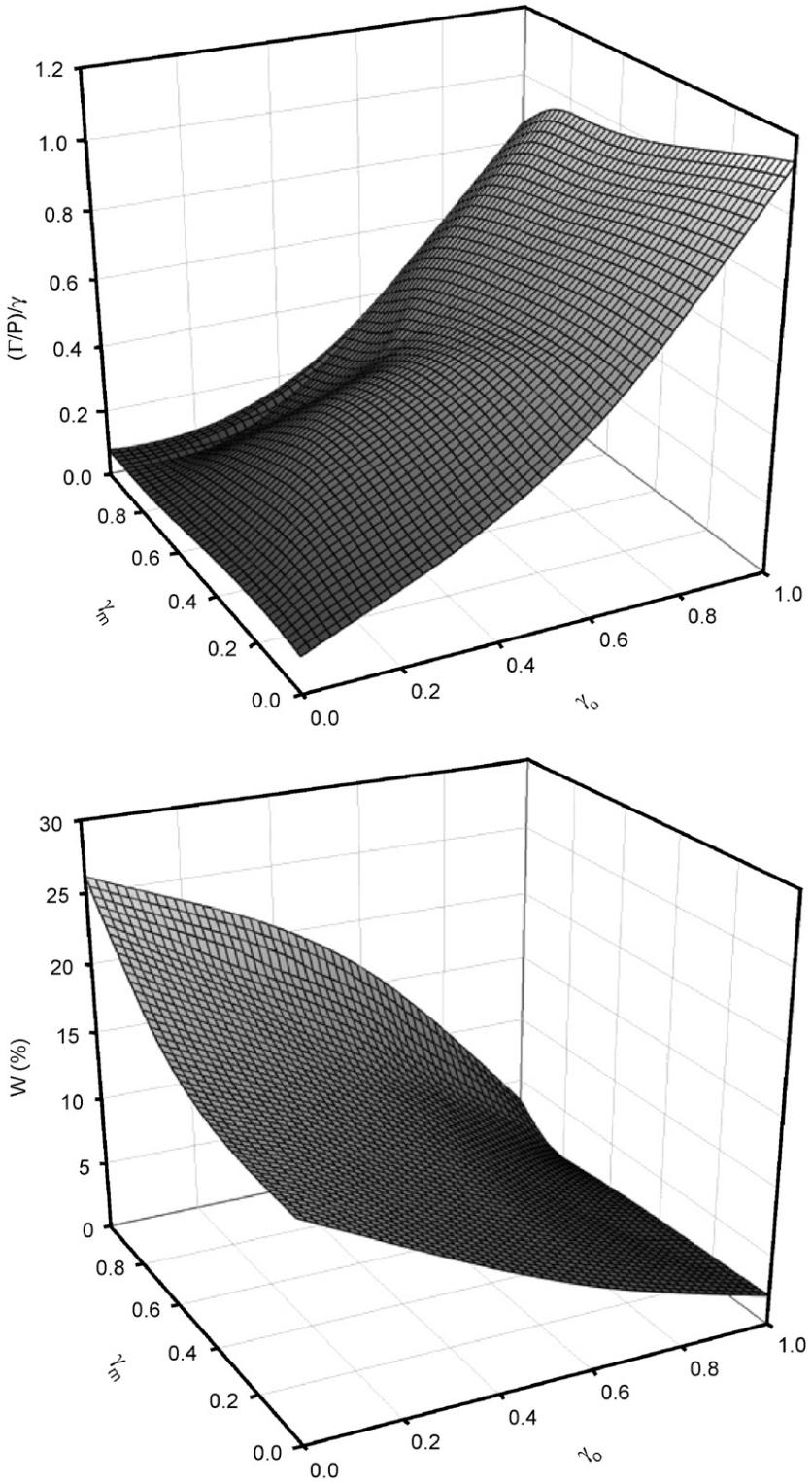

Fig. 9. Calculated broadening coefficients normalized by the asymptotic value and deviation parameters W as functions of the velocity memory parameters γ_{Ori} and γ_{Mod} for the $R(12)$ line at 0.1 atm.

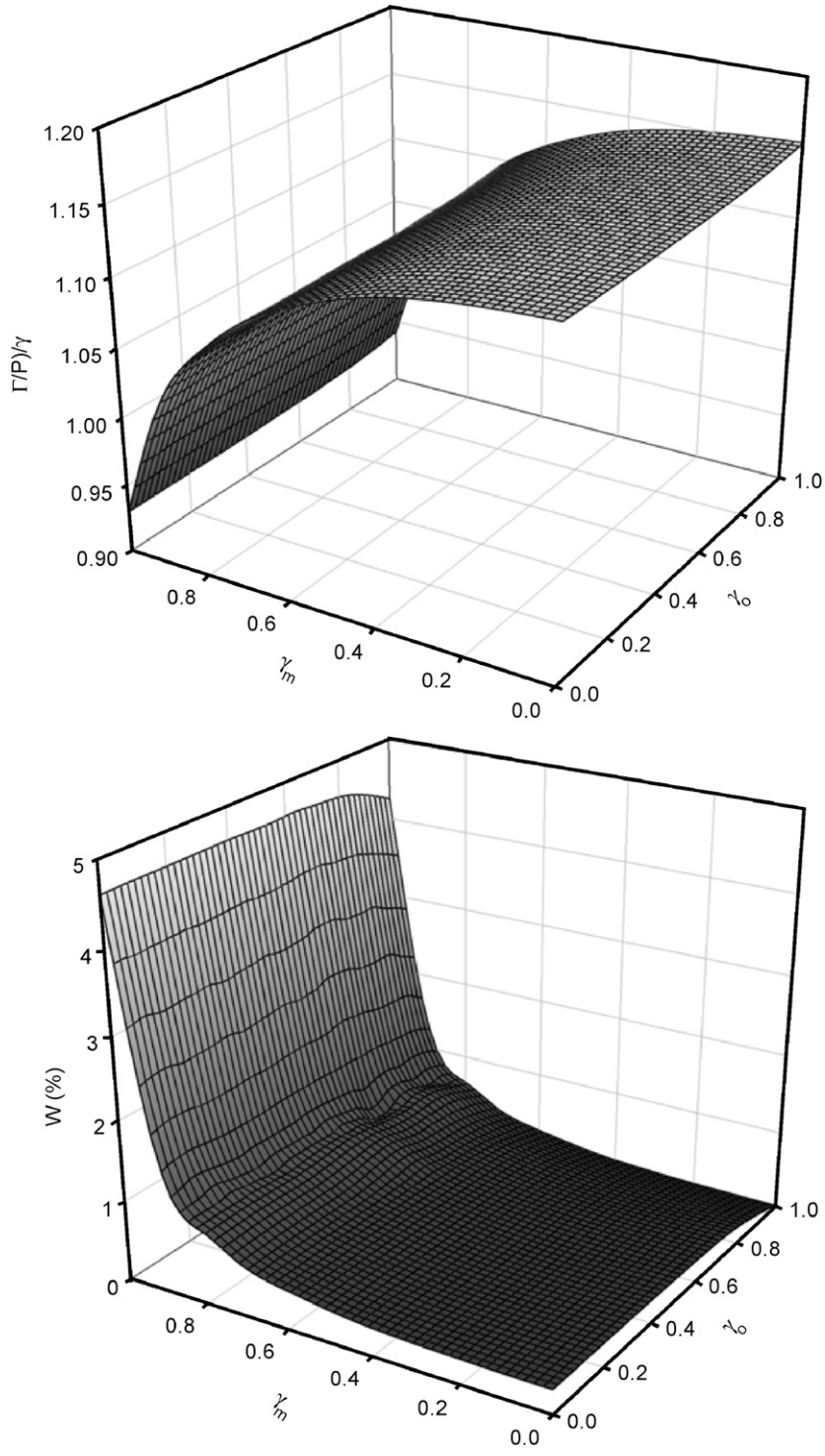

Fig. 10. Calculated broadening coefficients normalized by the asymptotic value and deviation parameters W as functions of the velocity memory parameters γ_{Ori} and γ_{Mod} for the $R(12)$ line at 2 atm.

are used, as shown in Fig. 11. Furthermore, the case $\gamma_{\mathrm{Ori}} = 0$ and $\gamma_{\mathrm{Mod}} = 1$ together with $\gamma(v) = \langle \gamma(v) \rangle$ and $\delta(v) = \langle \delta(v) \rangle$ corresponds to a speed-independent HC model. The results, plotted in Fig. 11 confirm that the speed dependence of collisional parameters is mostly responsible for the deviations from the

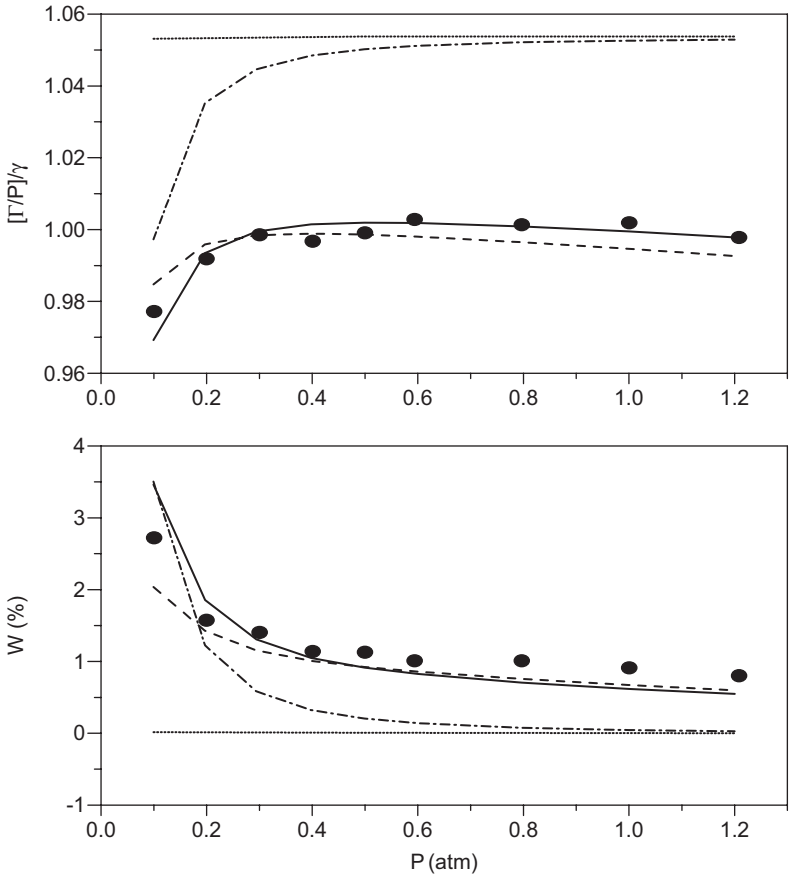

Fig. 11. Broadening coefficients normalized by the asymptotic value and deviation parameters W for the $R(3)$ line. ● are the experimental values whereas the various calculated results are obtained (see text) with —— $\gamma_{Ori} = 0.69$, $\gamma_{Mod} = 0.90$, $\gamma(v)$; - - - $\gamma_{Ori} = 1$, $\gamma_{Mod} = 1$, $\gamma(v)$; ⋯ ⋯ $\gamma_{Ori} = 1$, $\gamma_{Mod} = 1$, $\langle\gamma(v)\rangle$; ·–·– $\gamma_{Ori} = 0$, $\gamma_{Mod} = 1$, $\langle\gamma(v)\rangle$.

Voigt profile at elevated pressures; e.g. above about 0.4 atm in the case of the $R(3)$ line. On the contrary, the effects of changes of the orientation of the velocity (Dicke type narrowing) are only significant in the low-pressure range below about 0.2 atm for the $R(3)$ transition. This shows that the analysis of the narrowing made in many papers where it is entirely attributed to confinement through changes of the velocity orientation and the dependences of $\gamma(v)$ and $\delta(v)$ on v is neglected is clearly wrong. Hence, retrievals of the vertical profile of water vapor mixing ratios from high resolution and signal/noise ratio in situ measurements such as those of Ref. [43] cannot be done using usual (Voigt, HC, …) line-shapes. Their proper treatment over the pressure range of the troposphere and lower stratosphere requires a description of all processes including both velocity changes and the dependence of collisional parameters on speed.

Acknowledgements

One of the authors (RRG) is pleased to acknowledge the support for this research from the National Science Foundation (NSF) through Grant No. ATM-0242537. Any opinions, findings, and conclusions or recommendations expressed in this material are those of the author(s) and do not necessarily reflect the views of the National Science Foundation.

References

[1] Gamache RR, Hartmann JM. Collisional parameters of H_2O lines: effects of vibration. JQSRT 2004;83:119–47.
[2] Gamache RR, Hartmann JM. An intercomparison of measured pressure broadening and pressure shifting parameters of water vapor. Can J Chem 2004;82:1013–27.
[3] Eng RS, Calawa AR, Harman TC, Kelley PL, Javan A. Collisional narrowing of infrared water-vapor transitions. Appl Phys Lett 1972;21:303–5.
[4] Eng RS, Kelley PL, Mooradian A, Calawa AR, Harman TC. Tunable laser measurements of water vapor transitions in the vicinity of 5 μm. Chem Phys Lett 1973;19:524–8.
[5] Eng RS, Kelley PL, Calawa AR, Harman TC, Nill KW. Tunable diode laser measurements of water vapor absorption line parameters. Mol Phys 1974;28:653–64.
[6] Eng RS, Mantz AW. Tunable diode laser measurement of water vapor line parameters in the 10- to 15-μm spectral region. J Mol Spectrosc 1979;74:388–99.
[7] Grossmann BE, Browell EV. Spectroscopy of water vapor in the 720-nm wavelength region: line strengths, self-induced pressure broadenings and shifts, and temperature dependence of linewidths and shifts. J Mol Spectrosc 1989;136:264–94.
[8] Grossmann BE, Browell EV. Water-vapor line broadening and shifting by air, nitrogen, oxygen, and argon in the 720-nm wavelength region. J Mol Spectrosc 1989;138:562–95.
[9] Grossmann BE, Browell EV. Line-shape asymmetry of water vapor absorption lines in the 720-nm wavelength region. JQSRT 1991;45:339–48.
[10] Giesen T, Schieder R, Winnewisser G, Yamada KMT. Precise measurements of pressure broadening and shift for several H_2O lines in the v_2 band by argon, nitrogen, oxygen, and air. J Mol Spectrosc 1992;153:406–18.
[11] Avetisov VG, Nadezhdinskii AI, Khusnutdinov AN, Omarova PM, Zyrianov MV. Diode laser spectroscopy of water vapor in 1.8 μm: line profile measurements. J Mol Spectrosc 1993;160:326–34.
[12] Nagali V, Chou SI, Baer DS, Hanson RK. Diode laser measurements of temperature dependent half-widths of H_2O transitions in the 1.4 μm region. JQSRT 1997;57:795–809.
[13] Schmucker N, Trojan Ch, Giesen T, Schieder R, Yamada KMT, Winnewisser G. Pressure broadening and Shift of some H_2O lines in the v_2 band: revisited. J Mol Spectrosc 1997;184:250–6.
[14] Ponsardin PL, Browell EV. Measurements of H_2 ^{16}O linestrengths and air-induced broadenings and shifts in the 815-nm spectral region. J Mol Spectrosc 1997;185:58–70.
[15] Toth RA. Air- and N_2-broadening parameters of water vapor: 604 to 2271 cm^{-1}. J Mol Spectrosc 2000;201:218–43.
[16] Moretti L, Sasso A, Gianfrani L, Ciurylo R. Collisional-broadened and Dickenarrowed lineshapes of H_2 ^{16}O and H_2 ^{18}O transitions at 1.39 μm. J Mol Spectrosc 2001;205:20–7.
[17] Lepère M, Henry A, Valentin A, Camy-Peyret C. Diode-laser spectroscopy: line profiles of H_2O in the region of 1.39 μm. J Mol Spectrosc 2001;208:25–31.
[18] Claveau C, Henry A, Hurtmans D, Valentin A. Narrowing and broadening parameters of H_2O lines perturbed by He, Ne, Ar, Kr and nitrogen in the spectral range 1850–2140 cm^{-1}. JQSRT 2001;68:273–98.
[19] Claveau C, Henry A, Lepère M, Valentin A, Hurtmans D. Narrowing and broadening parameters for H_2O lines in the v_2 band perturbed by nitrogen from Fourier transform and tunable diode laser spectroscopy. J Mol Spectrosc 2002;212:171–85.
[20] Lisak D, Rusciano G, Sasso A. An accurate comparison of lineshape models on H_2O lines in the spectral region around 3 μm. J Mol Spectrosc 2004;227:162–71;
Lisak D, Hodges JT, Ciury o R. Comparison of semiclassical line-shape models to rovibrational H_2O spectra measured by frequency-stabilized cavity ring-down spectroscopy. Phys Rev A 2006;73:012507.
[21] Wagner G, Birk M, Gamache RR, Hartmann JM. Collisional parameters of H_2O lines: effect of temperature. JQSRT 2005;92:211–30.
[22] Bonamy L, Tran TNH, Joubert P, Robert D. Memory effects in speed-changing collisions and their consequences for spectral line shape. Eur Phys J D 2004;31:459–67.
[23] Tran H, Joubert P, Bonamy L, Lavorel B, Renard V, Chaussard F, et al. Femtosecond time resolved coherent anti-Stokes Raman spectroscopy: experiment and modelization of speed memory effects on H_2–N_2 mixtures in collision regime. J Chem Phys 2005;122:194317.
[24] Joubert P, Hoang PNM, Bonamy L, Daniel R. Speed dependence lineshape model analysis from molecular dynamic simulations: the collisional confinement narrowing regime. Phys Rev A 2002;66:042508.
[25] Domenech JL, PhD thesis, Madrid 1990.
[26] Santos J, Cancio P, Domenech JL, Rodriguez J, Bermejo D. Accurate wavenumber measurement in high-resolution stimulated Raman-spectroscopy (SRS) by using an infrared standard v_1 fundamental of $^{12}CH_4$. Laser Chem 1992;12:53–63.
[27] Gesternkorn S, Luc P. Atlas du Spectre d'absorption de la Molécule d'Iode 14 800–20 000 cm^{-1}. Editions du CNRS, Paris, 1978.
[28] Rothman LS, Jacquemart D, Barbe A, Benner DC, Birk M, Brown LR, et al. The HITRAN 2004 molecular spectroscopic database. JQSRT 2005;96:139–204.
[29] Zou Q, Varanasi P. Laboratory measurement of the spectroscopic line parameters of water vapor in the 950–2100 and 3000–4050 cm^{-1} regions at lower-tropospheric temperatures. JQSRT 2003;82:45–98.
[30] Mandin JY, Camy-Peyret C, Flaud JM. Measurements and calculations of selfbroadening coefficients of lines belonging to the v_2, v_1, and v_3 bands of H_2. Can J Phys 1982;60:94–101.

[31] Malathy Devi V, Benner DC, Smith MAH, Rinsland CP. Measurements of pressure broadening and pressure shifting by nitrogen in the v_1 and v_3 bands of $H_2{}^{16}O$. J Mol Spectrosc 1992;155:333–42.
[32] Remedios JJ, PhD dissertation. University of Oxford, 1990.
[33] Malathy Devi V, Fridovich B, Jones GD, Snyder DGS. Intensities and half-widths for several H_2O v_2 lines in the region 1500–1523 cm^{-1}. J Mol Spectrosc 1985;111:114–8.
[34] Yamada KMT, Harter M, Giesen T. Survey study of air-broadened water vapor lines in the v_2 band by high-resolution FTIR spectroscopy. J Mol Spectrosc 1993;157:84–94.
[35] Chang YS, Shaw JH. Intensities and widths of H_2O lines between 1800 and 2100 cm^{-1}. JQSRT 1977;18:491–9.
[36] Robert D, Bonamy L. Memory effects in speed-changing collisions and their consequences for spectral lineshape: I. Collision regime. Eur Phys J D 1998;2:245–52.
[37] Pickett HM. Effects of velocity averaging on the shapes of absorption lines. J Chem Phys 1980;73:6090–4.
[38] Abramowitz M, Stegun IA. Handbook of mathematical functions functions. New York: Dover Publications Inc.; 1970.
[39] Rautian SG, Sobel'man II. The effect of collisions on the Doppler broadening of spectral lines. Sov Phys Uspekhi 1967;9:701–16.
[40] Keilson J, Storer JE. On Brownian motion, Boltzmann's equation, and the Fokker–Planck equation. Quart Appl Math 1952;10:243–53.
[41] Burshtein AI, Temkin SI. Spectroscopy of molecular rotation in gases and liquids. Cambridge: Cambridge University Press; 1994.
[42] Hirschfelder JO, Curtis CF, Bird RB. Molecular theory of gases and liquids. New York: Wiley; 1964.
[43] Durry G, Zéninari V, Parvitte B, Le Barbu T, Lefèvre F, Ovarlez J, et al. Pressure broadening coefficients and line strengths of H_2O near 1.39 μm: application to the in situ sensing of the middle atmosphere with balloonborne diode lasers. JQSRT 2005;94:387–403.